CHAPTER 5 BULK PROPERTIES OF SCN

5.1 Summary

Here begins the second half of this thesis, focusing on bulk defect chemistry. Section 5.2 reviews the motivation presented in Chapter 1 for studying bulk defect chemistry in perovksites containing strontium and cobalt. Section 5.3 gives experimental details, Section 5.4 gives the results, and Section 5.5 reviews the findings.

5.2 Why study the bulk defect chemistry of $SrCo_{0.9}Nb_{0.1}O_{3-\delta}$ (SCN)?

In this chapter the oxygen nonstoichiometry, bulk impedance behavior, and expansion behavior of SCN are characterized. The oxygen nonstoichiometry and electronic behavior are clearly relevant to the catalytic behavior, while the expansion behavior is also interesting both from a theoretical perspective (since expansion is directly related to vacancy formation, electronic redistribution, etc.) and from an application perspective (since in applications, larger expansion typically leads to higher stresses and greater likelihood of crack formation at the cathode/electrolyte interface). SCN represents a reasonable choice of a "model material" for fundamental studies of SOFC catalysts with the perovskite structure that contain Sr and Co.

5.3 Experimental details

Phase-pure SCN powder was synthesized by conventional solid state reaction. Stoichiometric quantities of $SrCO_3$, Co_3O_4, and Nb_2O_5 (all from Alfa Aesar, > 99.7% purity) were mixed, attritor-milled at 500 rpm for 30 min with 3 mm yttria-stabilized zirconia beads in acetone or isopropanol, removed from the milling media, dried at 110˚C, and calcined for 15 h in stagnant air at 1200˚C. In some cases, powders were milled again and recalcined at 1200˚C an additional 10 h. For comparison, phase-pure powders with the nominal compositions $Ba_{0.5}Sr_{0.5}Co_{0.8}Fe_{0.2}O_{3-\delta}$ and $SrCoO_3$ were synthesized by a chemical solution method reported previously.[37] X-ray diffraction (XRD) (Philips X'Pert Pro, Cu Ka) confirmed that the calcined powders were cubic perovskites. To assess phase stability, a sample of this SCN powder was placed in an alumina boat in a quartz tube and subject to anneals in stagnant air for 750˚C for 4 days, then 750˚C for 6 more days, then 1200˚C for 10 h, with XRD patterns acquired after each of these anneals.

Dense compacts were prepared from powders to which 1.25 wt% polyvinylpyrrolidone was added to serve as a binder. The powders were subjected to uniaxial pressure under 2 tons for 10 min followed by isostatic pressure under 350 MPa for 20 min. Sintering was carried out at 1100˚C for 10 h in stagnant air. Prior to further characterization, the compact surfaces were polished using a final grit size of 0.3 mm. Electron microprobe (JEOL JXA-8200) analysis was employed for chemical analysis from a representative pellet of each composition, using $BaTiO_3$, $SrTiO_3$, Co, Fe, and Nb standards. At least six locations were probed, and the results were averaged. The relative cation amounts measured in the samples were converted into chemical formulas by assuming no interstitial cations and minimizing the number of cation vacancies. The resulting chemical formulas were $Ba_{0.50}Sr_{0.49\pm0.01}Co_{0.77\pm0.01}Fe_{0.21\pm0.01}O_{3-\delta}$ and $SrCo_{0.91\pm0.01}Nb_{0.09\pm0.01}O_{3-\delta}$. Micrographs taken using the same instrument indicated that the BSCF compacts had very little porosity; however, the SCN compacts were typically 30% - 55% porous. Accordingly all measured bulk resistances of SCN were multiplied by a correction factor to account for this porosity.

In all the measurements described below, the gas atmosphere was achieved by flowing premixed gases with various amounts of O_2 and N_2; the oxygen partial pressure of each gas composition was verified using a zirconia-based oxygen sensor (Setnag); measurements were typically made over an oxygen partial pressure range of 10^{-4} atm - 1 atm and over the temperature range 500˚C - 1000˚C (except 600˚C - 900˚C was used for the impedance measurements); and for each material and gas composition, the temperature was changed in 100˚C increments and measurements were taken continuously until equilibrium was reached. Equilibration times were 0.5 h - 2.5 h for powder samples and 0.5 h - 4 h for bar samples. BSCF exhibits a slow partial decomposition to a mixture of cubic and hexagonal phases[61-64], so samples of this material were frequently annealed at 1000˚C during the measurement sequence to restore the pure cubic phase.

Thermogravimetry (TG) measurements were performed on powder samples with a typical mass of 220 mg in a Netszch STA 449C thermal analyzer using a platinum crucible. The equilibrated sample masses were frequently re-measured at a "baseline condition" of 800˚C and 0.01 atm O_2 in order to monitor and correct for instrument drift (typically < 10 mg/h). Buoyancy- and drift-corrected mass changes between environmental conditions were attributed to changes in oxygen content; thus the relative oxygen stoichiometry at all conditions was determined. In order to translate the relative oxygen stoichiometries implied by these measurements into absolute stoichiometries, powder samples were heated to a reference state of 1000˚C in 0.20 atm O_2, and subsequently fully reduced (Ba,Sr)O + Co + Fe or SrO + Co + $SrNbO_3$ by exposure to inert gas and then 6-8% H_2. The mass difference at 1000˚C between the (equilibrated) reference state and the reduction products provided the absolute oxygen stoichiometry of the reference state. Complete reduction to the indicated products was verified using both *ex situ* XRD (on the reduction products) and *in situ* XRD (probing the reduction of a different sample under equivalent conditions). The reductions were performed twice for each material to verify reproducibility.

Bulk conductivity was measured using an impedance analyzer (Solartron 1260) and right rectangular prism samples of typical dimensions 23.5 mm × 5.4 mm × 0.25 mm. The samples were made thin so as to increase their resistance (thereby improving measurement accuracy) and surface-area-to-volume ratio (thereby decreasing equilibration times). Two sets of measurements were performed. In the first set, data were collected on BSCF over the frequency range 10^{-2} Hz to 10^{7} Hz with zero d.c. bias and 10 mV - 40 mV perturbation voltage. Porous platinum ink (BASF A3788) was spread on the distant ends of the compact, fired at 950˚C for 2 h, and verified by scanning electron microscopy (SEM, Hitachi S-4100) to be porous and uniform. Electrical contact was made to the platinum using gold wires attached with silver paste (SPI 05063-AB). A second set of measurements was performed on both materials with the platinum paste omitted and at a fixed frequency of 100 Hz (again with zero d.c. bias and 10 mV - 40 mV perturbation voltage). Short circuit measurements were made to measure and correct for the resistance of the experimental apparatus. The total electrical conductivity was calculated from the corrected sample resistance (typically 1 W - 40 W) and the sample geometry.

The expansion behavior of SCN was measured by taking *in situ* x-ray diffraction patterns (Philips X'Pert Pro, Cu Ka) on a bulk powder sample supported by an alumina cup and equilibrated in various environmental conditions in an Anton-Paar HTK 1200 chamber. The lattice parameter a_0 of SCN at each measured condition was determined from the corresponding diffraction pattern using a Nelson-Riley plot[65]. After the experiment, the alumina cup was observed to have a slight bluish tinge, indicating a very minor degree of interfacial reactivity between SCN and the alumina. However, this reactivity could be neglected; the bottom of the alumina cup where the interfacial reaction occurred was two orders of magnitude deeper than the x-ray penetration length.

5.4 Results and discussion

After calcining, SCN was found to have the cubic perovskite crystal structure at 25˚C. By contrast, $SrCoO_3$ was found to have segregated into two phases at 25˚C, $Sr_6Co_5O_{15}$ and Co_3O_4, consistent with literature findings.[66] Upon annealing at 750˚C for 10 d, SCN remained mostly in the cubic perovskite phase, but exhibited additional reflections that were indexable to the phases $Sr_6Co_5O_{15}$ and Co_3O_4, as shown in Figure 5.1. This decomposition was reversed by re-annealing at 1200˚C, as shown. Additional TG measurements (not shown) involving repeated temperature cycles between 1000˚C and 750˚C found that re-annealing at 1000˚C was sufficient to reversed the slow mass change observed at 750˚C, and that the mass was stable with time at 1000˚C. These results indicate that the 10% niobium doping in SCN successfully stabilizes the cubic perovskite phase at 1000˚C, however at lower temperatures this phase is metastable. Similarly, BSCF powder was also found to be stable at 950˚C and metastable at 750˚C. The impact of the metastability was minimized in the *in situ* studies reported below by frequently annealing the SCN (or BSCF) at 1000˚C to restore the cubic phase.

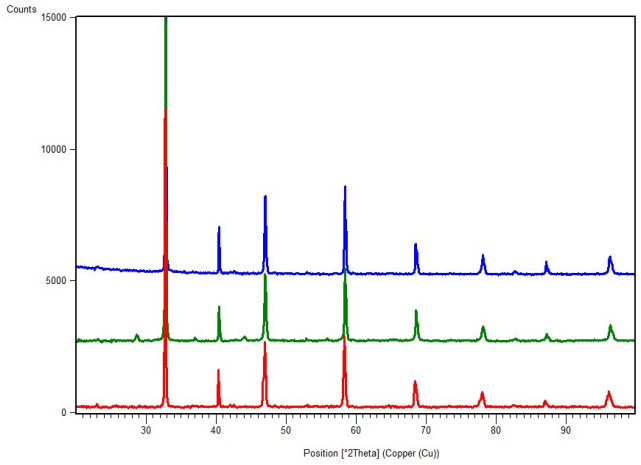

Figure 5.1. X-ray powder diffraction patterns for SCN after calcination at 1200˚C (red), after a subsequent anneal at 750˚C in air for 10 d (green), and after a subsequent additional anneal at 1200˚C in air for 10 h (blue).

The oxygen stoichiometry diagrams deduced from the thermogravimetry results are presented in Figure 5.2. Selected literature data are shown for comparison. The trends with temperature and oxygen partial pressure are quite similar between the two materials, apparently due to the cobalt ion.

Multiple reports of the oxygen stoichiometry phase diagram of BSCF exist in the literature.[63,67-69] The trends with temperature and oxygen partial pressure are consistent across these reports, but the absolute values differ substantially, apparently due to discrepancies in the reference state measurements. The BSCF reference state obtained in this study using thermogravimetry is identical to that obtained in a recent report by Kriegel *et al.*[63] that employed cerimetric titration. By contrast, Mueller *et al.* found a different reference point by a novel coulometric titration method, however it is not clear that their conclusion should be considered

definitive, since it appears to be based on a single data point from a single titration curve.[69]

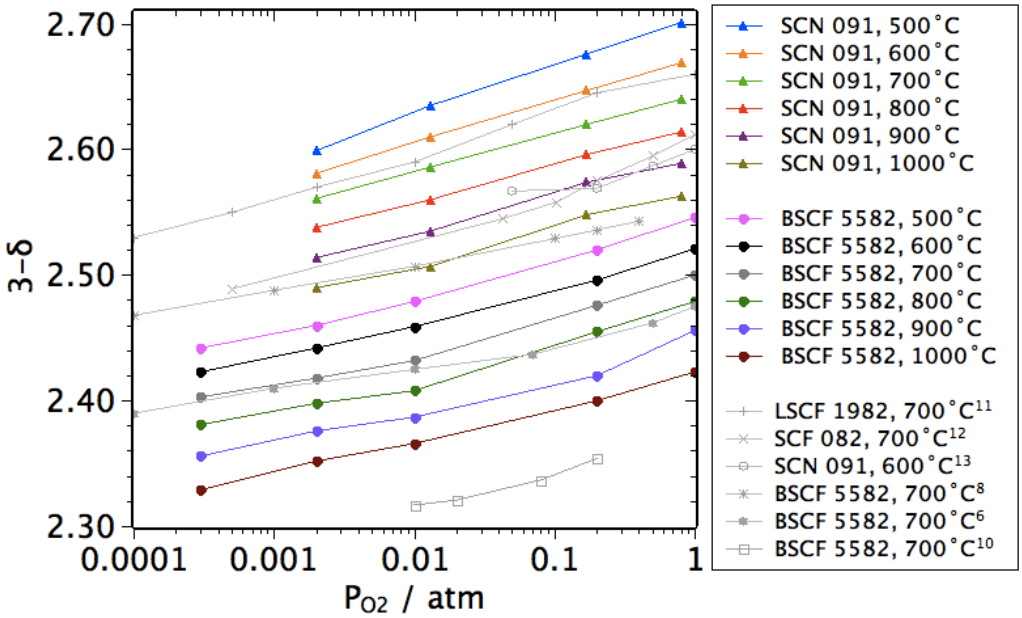

Figure 5.2. Oxygen stoichiometry 3-δ of BSCF and SCN measured by thermogravimetry, plotted for comparison with data from other reports on $La_{0.1}Sr_{0.9}Co_{0.8}Fe_{0.2}O_{3-\delta}$ (LSCF 1982)[70], $SrCo_{0.8}Fe_{0.2}O_{3-\delta}$ (SCF 082)[71], SCN[72], and BSCF[63,67,69].

Mueller *et al.* suggested some plausible sources of error in earlier studies that could account for the reference state discrepancies.[69] One consideration is worth adding to their excellent discussion: it appears that some earlier studies used a sample at room temperature as a reference point. This practice is potentially unreliable, because differences in oxygen uptake can occur between samples that are cooled to room temperature at different rates or with different geometries, or even between two powder samples taken from the surface and

interior of the same pile of powder. Thus, a metastable reference sample can be non-representative of other metastable test samples. This problem can be solved by choosing a reference state where the material is in stable equilibrium. Additionally, surface carbonates can form during powder storage due to a slow reaction with ambient carbon dioxide, and the subsequent burning off of the carbon during thermogravimetric analysis causes an additional mass loss that may be incorrectly interpreted as oxygen loss, thus leading to a calculated 3-δ value for the reference state that is too large. Again the solution is to choose a high temperature reference state at which carbonates are not present.

Note also that for this type of compound, common chemical analysis techniques have an uncertainty of at least 1% - 2% in determining any given cation ratio, thereby contributing additional uncertainty to the reference state calculation. In the present study, $BaTiO_3$ and $SrTiO_3$ were used as elemental standards, since using standards with similar crystal structure as the sample helps to maximize the accuracy of electron probe microanalysis.

Given all these considerations, error bars for the oxygen stoichiometry values measured in this paper are estimated as ±0.10 (absolute) and ±0.02 (relative for each material).

Turning to the transport behavior, the complex impedance of the platinum-electroded BSCF compact was constant with negligible imaginary component over the frequency range 10^{-1} Hz - 10^{5} Hz. A very small electrode arc was observed in the range 10^{-3} Hz - 10^{-1} Hz, which contributed to the overall DC resistance by less than 3%. These measurements include contributions from both electron and

oxygen ion carriers, but the negligible contribution of the electrode arc and the high total conductivity indicate that electronic transport is dominant with a transference number close to one.[26] This result is not surprising; the $La_{1-x}Sr_xCo_{1-x}Fe_xO_{3-\delta}$ family of materials also have electronic transference numbers approaching unity.[3] Accordingly, the total electrical conductivity can be equated with negligible loss of accuracy to the electronic conductivity, and single frequency measurements are justified.

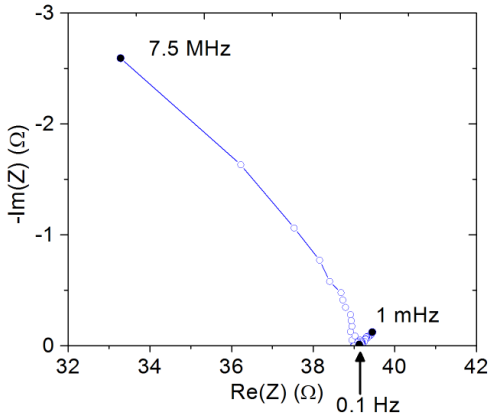

Figure 5.3. Impedance spectrum of $Ba_{0.5}Sr_{0.5}Co_{0.8}Fe_{0.2}O_{3-\delta}$ at 600˚C in $2x10^{-5}$ atm O_2.

The electronic conductivity of BSCF and SCN are plotted in Figure 5.4 as isotherms and isobars. Selected literature data are again included for comparison. As the oxygen partial pressure increases along the isotherms, oxygen atoms are incorporated (Figure 5.2), and in becoming ions they pull electrons from other ions in the material. The electronic conductivities are seen to increase, so holes are the majority carrier; that is, both materials are p-type.

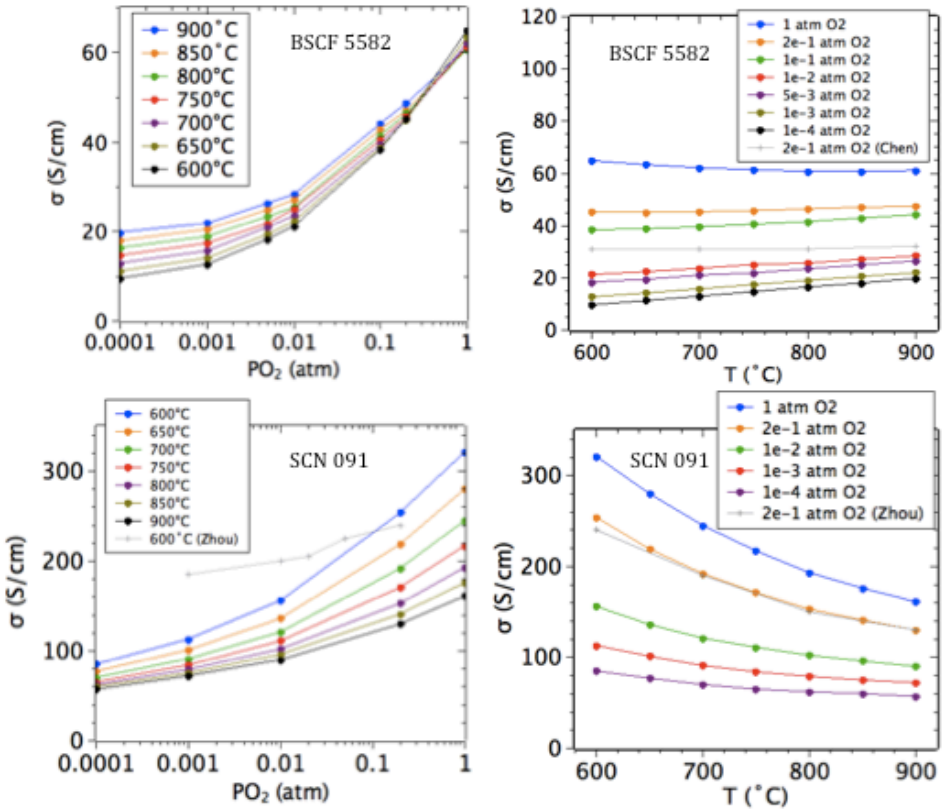

Figure 5.4. Electronic conductivity σ. (a) BSCF isotherms, (b) BSCF isobars, (c) SCN isotherms, and (d) SCN isobars, plotted with comparable literature data.[72,73]

Along some of the isobars, the electronic conductivity decreases as temperature increases. In many materials such a trend suggests metallic behavior, *i.e.*, itinerant carriers whose mobility is reduced at higher temperatures due to increased phonon scattering. One previous report did indeed claim on the basis of this trend that BSCF exhibits metallic behavior.[74] In these materials, however, conclusions about mobility and transport mechanisms can only be legitimately drawn after accounting for changes in carrier concentration due to redox reactions. Here we access the desired "iso-stoichiometric" values of conductivity by assuming that fixed oxygen stoichiometry corresponds to fixed carrier concentration. In other words, we neglect changes of the mobile carrier concentration with temperature due to disproportionation reactions (*e.g.*, $2Co^{3+} \rightarrow Co^{2+} + Co^{4+}$) and internal charge transfer reactions (*e.g.*, $Fe^{3+} + Co^{4+} \rightarrow Fe^{4+} + Co^{3+}$). While this assumption may not be entirely justified, the relatively small temperature range of the analysis limits the associated error; the assumption is a possible source of error for the calculated $\Delta_m H$ values, but it seems unlikely to undermine the overall conclusions drawn below.

It can be shown that materials with hopping conductivity and fixed electronic carrier concentrations exhibit Arrhenius behavior, *i.e.*, satisfy the expression

$$\ln(\sigma T) = \ln(C) + \frac{\Delta_m H}{k_B T} \qquad (3)$$

where σ is the electronic conductivity, T is temperature, $\Delta_m H$ is the enthalpy of hole migration (*i.e.*, the activation energy for hole hopping between sites), k_B is

Boltzmann's constant, and C is a constant accounting for the entropy of hole migration $\Delta_m S$ and other terms.[75] Figure 5.5 shows log(σ*T) plotted as a function of T^{-1} while keeping δ fixed; this figure combines the oxygen stoichiometry and electronic conductivity results shown earlier. Specifically, linear fits to the isotherms in Figure 5.2 and parabolic fits to the isotherms in Figure 5.4 (all of which showed good agreement with the data) were used to interpolate those data and thereby produce the points in Figure 5.5.

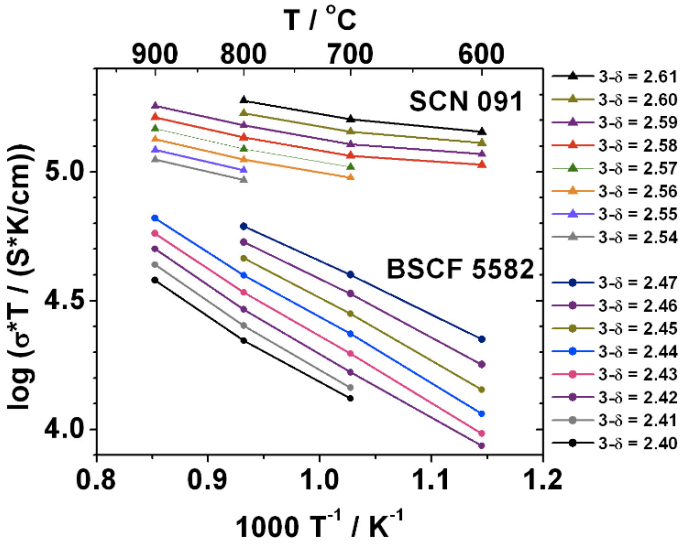

Figure 5.5. Electronic conductivity σ of BSCF and SCN plotted as iso-stoichiometric curves. Lines connect the data points as guides for the eye.

For fixed carrier concentration, conductivity clearly increases with increasing temperature for both SCN and BSCF, indicating that under the conditions studied, these materials are not metallic conductors; rather, they are thermally activated conductors with localized holes. From the slopes in the above plot, the enthalpy of migration $\Delta_m H$ is found to be 0.4 eV - 0.5 eV for BSCF and 0.1 eV - 0.2 eV for SCN.

These values are physically plausible, and for comparison, the enthalpy of electron migration in $Sm_{0.15}Ce_{0.85}O_{1.925-\delta}$ (a material that is well-known to conduct electrons by small polaron hopping) is 0.2 eV.[26]

Turning finally to the expansion behavior, Figure 5.6 shows the lattice parameter a_0 of SCN measured using *in situ* XRD as a function of temperature and oxygen partial pressure. Comparable literature data for BSCF (taken using *in situ* neutron diffraction) are shown for comparison. The same SCN lattice parameter data are plotted (again alongside comparable literature data for BSCF) in Figure 5.7 as a function of δ and temperature, where the values of δ were determined by interpolating linear fits to the isotherms in Figure 5.2.

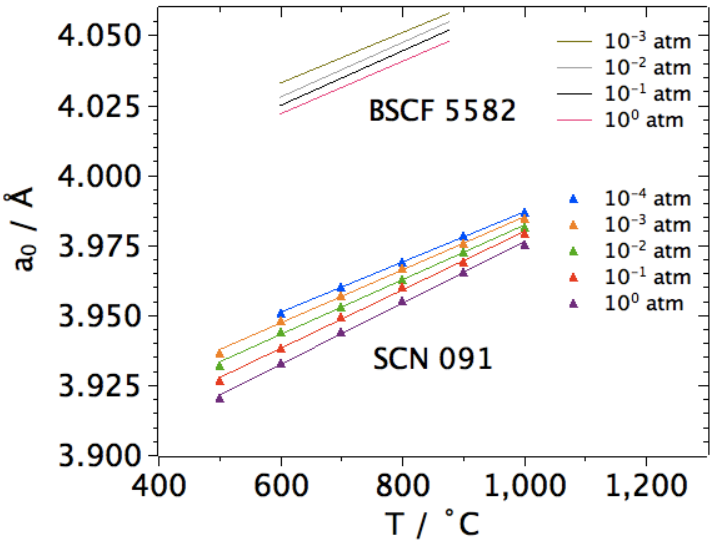

Figure 5.6. Lattice parameter a_0 of equilibrated SCN measured by *in situ* x-ray diffraction. Curves shown are linear fits to the data. Also plotted are comparable literature data for equilibrated BSCF taken by neutron diffraction.[68]

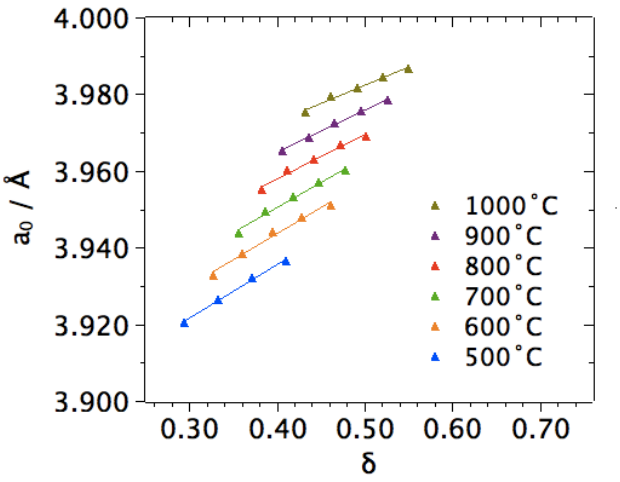

Figure 5.7. Lattice parameter a_0 of equilibrated SCN, plotted as a function of oxygen non-stoichiometry δ. Curves shown are linear fits to the data. Error bars for d are estimated as ±0.10 (absolute) and ±0.02 (relative).

From these data the linear expansivity a_l, the linear chemical expansivity a_c, and the linear thermal expansivity a_t can be determined by

$$\alpha_l \equiv \frac{1}{l}\left(\frac{\partial l}{\partial T}\right)_{P_{O_2}} = \frac{1}{a_0}\left(\frac{\partial a_0}{\partial T}\right)_{P_{O_2}} \tag{4}$$

$$\alpha_c \equiv \frac{1}{l}\left(\frac{\partial l}{\partial \delta}\right)_{T} = \frac{1}{a_0}\left(\frac{\partial a_0}{\partial \delta}\right)_{T} \tag{5}$$

$$\alpha_t \equiv \frac{1}{l}\left(\frac{\partial l}{\partial T}\right)_{\delta} = \frac{1}{a_0}\left(\frac{\partial a_0}{\partial T}\right)_{\delta} \approx \left(\frac{\Delta(\ln a_0)}{\Delta T}\right)_{\delta} \tag{6}$$

where a_0 and l are the lattice parameter and macroscopic length. The first definition is standard;[76] the latter two definitions are linear versions of the volumetric expansivities described by Adler.[77] Note that linear expansivity includes the effects of both thermal and chemical expansion, and thus is sometimes

referred to as the total expansion coefficient. Note also that the unit cell is assumed to be uniform throughout the sample, so that macroscopic expansion (changes in l) and unit cell expansion (changes in a_0) can be taken as equivalent. Thus it is possible to calculate a_l from the slopes of the isobars in Figure 5.6, a_c from the slopes of the isotherms in Figure 5.7, and a_t from applying Equation 6 to adjacent points with the same δ in Figure 5.7. The results for a_l and a_c are shown in Figure 5.8 and Figure 5.9, and a_t for SCN was determined to be $a_t = (18 \pm 2)*10^{-6}$ K^{-1} over the range of conditions studied; it showed no clear trend with temperature or δ. For comparison, the thermal expansivity of BSCF is reported to be $(20 \pm 1)*10^{-6}$ K^{-1} over a comparable range of conditions.[68]

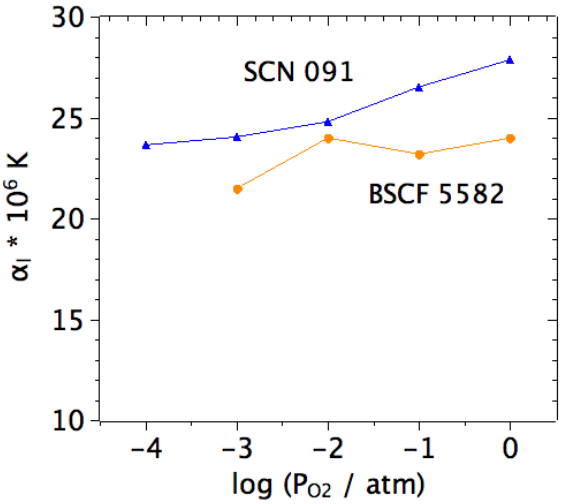

Figure 5.8. Linear expansivity a_l of SCN plotted with comparable literature data for BSCF.[68]

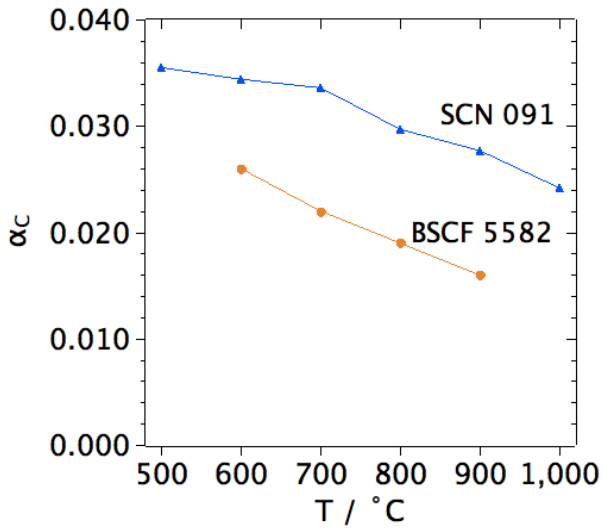

Figure 5.9. Linear chemical expansivity a_C of SCN plotted with comparable literature data for BSCF.[68]

These results indicate that the thermal expansivities of the two materials are comparable, and that SCN has a larger chemical expansivity and thus a slightly larger total expansivity than BSCF.

As an aside, a recent computational study on $CeO_{2-\delta}$ and $BaCeO_{3-\delta}$ suggested that materials with smaller degree of charge localization have smaller a_c.[78] However the comparison of SCN and BSCF appears to provide a counterexample, since SCN has a smaller degree of charge localization (smaller $\Delta_m H$) but a larger a_c than BSCF.

5.5 Conclusions

SCN is metastable at fuel cell operating temperatures. The kinetics of decomposition are fairly slow, however, and contribute minimal error on the time scale of many laboratory measurements. SCN is a thermally activated hole

conductor, and in comparison with the current state-of-the-art material, $Ba_{0.5}Sr_{0.5}Co_{0.8}Fe_{0.2}O_{3-\delta}$ (BSCF), SCN has smaller oxygen nonstoichiometry, five times higher electronic conductivity, lower enthalpy of hole migration, somewhat improved structural stability, comparable thermal expansivity, and slightly larger total and chemical expansivities.